

Zirconium silicates in a peralkaline granite: a record of the interplay of magmatic and hydrothermal processes (Ilímaussaq complex, Greenland)

MAŁGORZATA CEGIELKA^{1,2}, BOGUSŁAW BAGIŃSKI^{1,*}, RAY MACDONALD^{1,3}, HARVEY E. BELKIN⁴,
JAKUB KOTOWSKI¹ and BRIAN G.J. UPTON⁵

¹ Department of Geochemistry, Mineralogy and Petrology, Faculty of Geology, University of Warsaw,
ul. Żwirki i Wigury 93, 02-089 Warsaw, Poland.

E-mails: B.Baginski1@uw.edu.pl; j.kotowski@uw.edu.pl

² Institute of Geological Sciences, Polish Academy of Sciences, Research Centre in Warsaw,
ul. Twarda 51/55, 00-818 Warsaw, Poland.

E-mail: m.cegielka@twarda.pan.pl

³ Environment Centre, Lancaster University, Lancaster LA1 4YQ, UK.

E-mail: raymacdonald186@gmail.com

⁴ 11142 Forest Edge Drive, Reston, VA 20190, USA.

E-mail: harveybelkin@gmail.com

⁵ Grant Institute, University of Edinburgh, James Hutton Rd., Edinburgh EH9 3FE, UK.

E-mail: brian.upton@ed.ac.uk

* Corresponding author

ABSTRACT:

Cegielka, M., Bagiński, B., MacDonald, R., Belkin, H.E., Kotowski, J. and Upton, B.G.J. 2022. Zirconium silicates in a peralkaline granite: a record of the interplay of magmatic and hydrothermal processes (Ilímaussaq complex, Greenland). *Acta Geologica Polonica*, **72** (2), 235–245. Warszawa.

Compositional and textural data are presented for zircon, secondary Zr-silicates, catapleiite and elpidite in a peralkaline granite from the Ilímaussaq complex, south Greenland. The zircon is essentially stoichiometric, with $(Zr + Hf + Si) = 1.96\text{--}1.98$ a.p.f.u. The secondary Zr-silicates show a wide range of Zr/Si atomic ratios (0.13–0.79). The catapleiite varies from close to stoichiometric to a Na-depleted type showing cation deficiency (5.2–5.8 a.p.f.u.). Elpidite shows similar variations (7.2–9.0 a.p.f.u.). Textural relationships between the Zr phases are interpreted to show that magmatic zircon interacted with hydrous fluids exsolved from the magma to form the secondary Zr-silicates. Formation of catapleiite was late-magmatic, in equilibrium with a Na-Si-bearing fluid. This was followed by the crystallization of elpidite, the fluid having a different Na/Si ratio. Both catapleiite and elpidite experienced Na-loss during late-stage hydrothermal alteration.

Key words: Peralkaline granite; Ilímaussaq complex; Zircon; Catapleiite; Elpidite; Hydrothermal fluids.

INTRODUCTION

Zircon is the dominant Zr-bearing phase in granitic rocks s.l. and miaskitic syenites. On the other hand, peralkaline and agpaitic rocks contain, in addition to zircon, a variety of Na-Ca-Zr silicates (Table 1).

Some mineral varieties remain unidentified (e.g., Andreeva 2016; Estrade *et al.* 2018). The alteration of Zr-silicates is most commonly ascribed to interaction with hydrous melts or to late- or post-magmatic aqueous fluids in the final stages of crystallization. During alteration, the minerals can show complex re-

Zr-silicate		Formula
Zircon		ZrSiO ₄
Na-phases	Catapleiite	Na ₂ ZrSi ₃ O ₉ ·2H ₂ O
	Elpidite	Na ₂ ZrSi ₆ O ₁₅ ·3H ₂ O
Ca-phases	Gittinsite	CaZrSi ₂ O ₇
	Armstrongite	CaZrSi ₆ O ₁₅ ·2H ₂ O
	Eudialyte	Na ₁₅ Ca ₆ Fe ₃ Zr ₃ Si(Si ₂₅ O ₇₃)
Unnamed phases	Yttrium zirconosilicate ¹	formula not given
	Ca-Na zirconosilicate ²	formula not given

Table 1. Zr-silicates referred to in the text. ¹ Andreeva 2016; ² Estrade *et al.* 2018.

wt. %			ppm		ppm		ppm
SiO ₂	73.35	Ba	51	Th	29.8	Ho	4.53
TiO ₂	0.21	Be	24	U	7.7	Er	12.3
Al ₂ O ₃	10.85	Co	36.5	V	<8	Tm	1.67
Fe ₂ O ₃ *	4.38	Cs	2.50	W	558	Yb	10.16
MnO	0.09	Ga	35.6	Zr	572	Lu	1.39
MgO	0.04	Hf	14.7	La	174	Y	142
CaO	0.52	Nb	140	Ce	341		
Na ₂ O	4.55	Ni	<20	Pr	37.6		
K ₂ O	4.84	Rb	454	Nd	138		
P ₂ O ₅	0.02	Sc	<1	Sm	24.6		
LOI	0.8	Sn	10.0	Eu	1.31		
TOT/C	0.14	Sr	20.2	Gd	21.7		
Total	99.79	Ta	13.1	Dy	21.3		

Table 2. Chemical composition of the Green Granite. Fe₂O₃*, all Fe as Fe³⁺.

placement relationships, the replacement sequences being related, *inter alia*, to pressure, temperature, the F and Cl concentrations, as well as Ca/Na ratios in the hydrothermal fluids. Several such sequences have been recorded in peralkaline granites. In the Strange Lake complex, Canada, Salvi and Williams-Jones (1995) recorded primary elpidite being replaced by post-magmatic gittinsite and armstrongite. Kynický *et al.* (2011) described the sequence Ca-poor elpidite → Ca-rich elpidite → minor gittinsite and abundant zircon in the Khan Bogd complex, southern Mongolia. In a metasomatite from the Khalzan Buregte deposit, Western Mongolia, Kempe *et al.* (2015, Fig. 12) described gittinsite enclosed in calciocatapleiite and replaced by zircon. In the so-called transitional granite of the Ambohimirahavavy complex, Madagascar, eudialyte-group minerals (EGM) were partly to totally replaced by zircon and quartz, while in the agpaite granites in the same complex the EGM were replaced by an unidentified Ca-Na-zirconosilicate (Estrade *et al.* 2018).

In this study of a peralkaline granite from the Gardar alkaline province, Greenland, we describe the replacement of magmatic zircon by an altered variety and the crystallization of catapleiite and then

elpidite, with a final stage of hydrothermal alteration affecting the zirconosilicates. We propose an evolutionary sequence involving interaction of magmatic phases and fluids of variable composition. Unlike in the cases listed above, EGM were not formed, perhaps because the melt Ca/Na ratio (0.06) and Cl content were too low to stabilize them (Table 2).

GEOLOGICAL SETTING

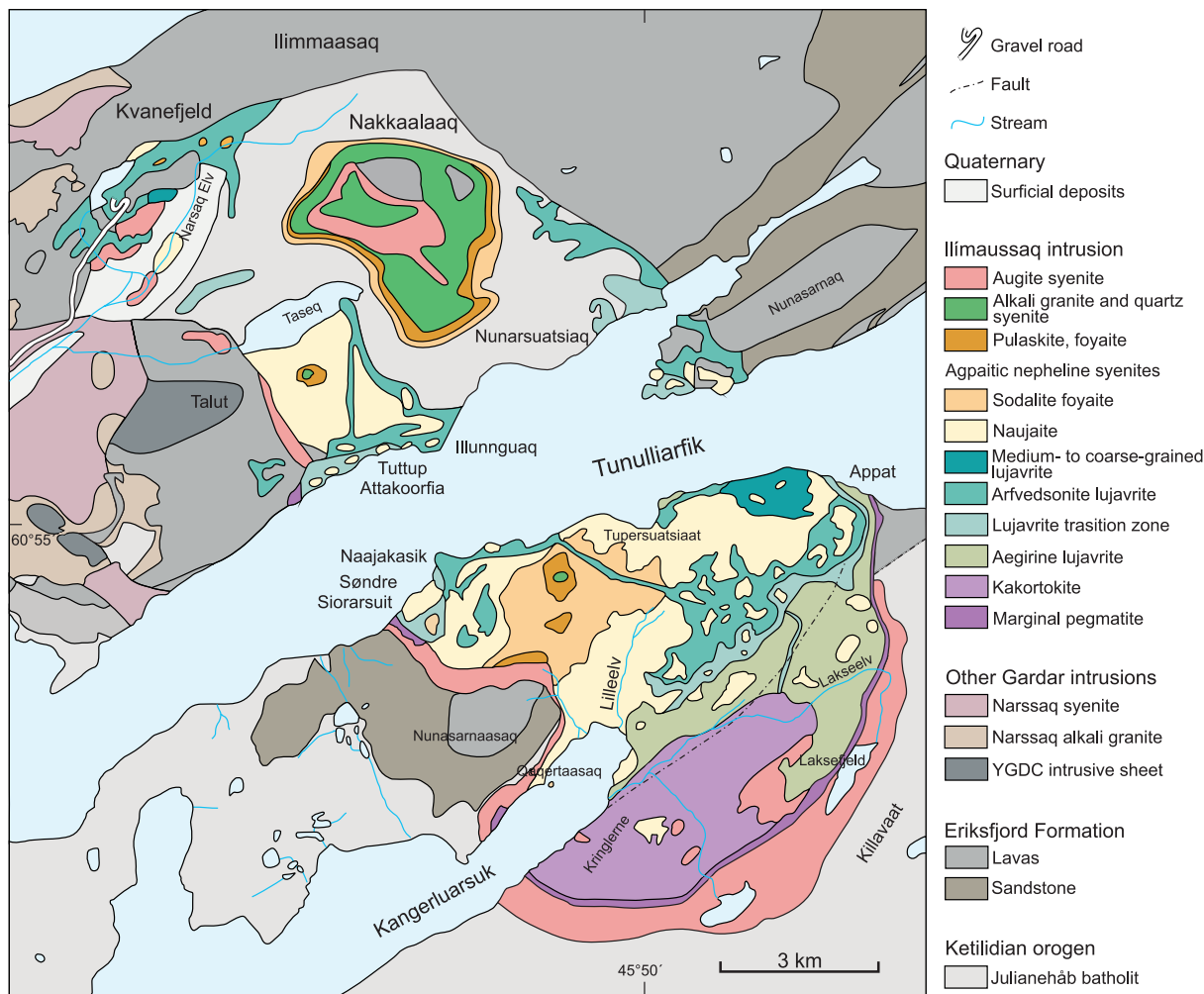
The Ilímaussaq alkaline complex (1161 ± 5 Ma; Krumrei *et al.* 2006), consists of four main intrusive phases (Text-fig. 1). Phase 1 is a partial rim of augite syenite, Phase 2 is peralkaline granite and quartz syenite, Phase 3 is foyaite, naujaite and pulaskite, and Phase 4 consists of kakortokites and lujavrites (Sørensen 2006; Sørensen *et al.* 2006; Marks and Markl 2015). Phases 3 and 4 comprise the agpaite suite.

Field studies demonstrated that xenoliths of quartz syenite and alkali granite occur in the uppermost facies of the agpaite suite (Steenfelt 1981). The augite syenite was intruded by sheets of alkali granite and alkali quartz syenite, with the development of chilled margins in the latter (Hamilton 1964; Steenfelt 1981). The intrusion of both the quartz syenite and granite probably occurred in more than one pulse, the larger sheets representing separate magmatic intrusions (Hamilton 1964; Steenfelt 1981).

ANALYTICAL METHODS

Our sample was collected from a loose block in the Dyrnaes River. From its intense green colour and mineralogy, the sample is undoubtedly from the Ilímaussaq peralkaline granite, the so-called Green Granite. A whole-rock analysis of the sample was made at Bureau Veritas Commodities Canada Ltd (more details are given at the website: <https://commodities.bureauveritas.com/metals-minerals/mineral-processing/analytical-services>). Major elements and Cr were analysed by ICP-ES, and trace elements, including REE, by ICP-MS. Mean detection limits on major elements were close to 0.1 wt.% whilst the detection limits for trace elements varied from 0.01 to 0.1 ppm.

Mineral compositions were determined in the Inter-Institution Laboratory of Microanalysis of Minerals and Synthetic Substances (Faculty of Geology, University of Warsaw), using Cameca SX100 and SXFiveFE microanalyzers equipped with four and five wavelength dispersive spectrometers (WDS), re-



Text-fig. 1. Geological map of the Ilimaussaq complex, modified from Upton (2013).

spectively. The operating conditions of the electron microprobe were: 15 kV accelerating voltage, 5–20 nA probe current and focused or defocused (even up to 20 μm in diameter) electron beam. Details of the microprobe analysis (e.g. emission lines, standards, diffracting crystals, detection limits) are listed in the Appendices. The $\varphi(\rho Z)$ correction model (X-PHI in the microprobe software) developed by Merlet (1994) was used for corrections.

THE GREEN GRANITE

The granite is holocrystalline, porphyritic and massive rock without any visible orientation of crystals. The dominant phase is subhedral alkali feldspar (55 modal %; 2–4 mm in size), comprising potassic feldspar (26 %; $\text{Ab}_{1.57}\text{Or}_{98.43}$) and sodic feldspar (29%;

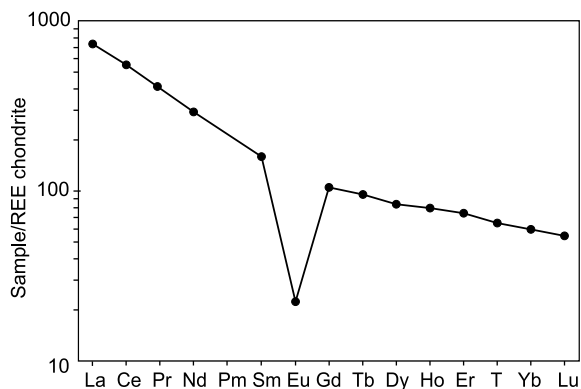
$\text{Ab}_{99.52}\text{Or}_{0.41}\text{An}_{0.07}$). Both types of feldspar contain aegirine inclusions ranging from 5 to 30 μm in size. These are probably the cause of the remarkable green colour of the rock. Anhedronal quartz, often showing undulose extinction, forms over 35 % of the granite, the grain size ranging from 60 μm to 5 mm. Amphiboles are the most abundant mafic minerals (8 modal %), forming large (40 μm to 6 mm) crystals with a zonation ranging from deep reddish-brown, richteritic, cores through light brownish-green to dark bluish-green, arfvedsonitic, margins. Aenigmatite occurs as deep-brown anhedronal crystals, up to 3 mm in size, commonly mantled by aegirine, titanite and fluorite.

The rock contains a large number of accessory minerals (Table 3), which occupy ~1 modal % in total: aegirine, astrophyllite, britholite-(Ce), catapleite, chevkinite-(Ce), ekanite, elpidite, fluorite, henrymeyerite, Fe-poor Ba-titanate, ilmenite, leucosphenite, loren-

Mineral	Formula
Aegirine	$\text{NaFe}^{3+}\text{Si}_2\text{O}_6$
Astrophyllite	$\text{K}_2\text{NaFe}^{2+}_7\text{Ti}_2\text{Si}_8\text{O}_{26}(\text{OH})_4\text{F}$
Britholite-(Ce)	$(\text{Ce,Ca})_5(\text{SiO}_4)_3\text{OH}$
Chevkinite-(Ce)	$(\text{Ce,L a,C a,Th})_4(\text{Fe}^{2+},\text{Mg})(\text{Fe}^{2+},\text{Ti,Fe}^{3+})_2(\text{Ti,Fe}^{3+})_2(\text{Si}_2\text{O}_7)_2\text{O}_8$
Ekanite	$\text{Ca}_2\text{ThSi}_8\text{O}_{20}$
Fe-poor Ba-titanate	$(\text{Ba,C a,N a})(\text{Ti,Fe}^{2+},\text{Nb})_5\text{O}_{11}$
Fluorite	CaF_2
Henrymeyerite	$\text{Ba}(\text{Ti}^{4+}_7\text{Fe}^{2+})\text{O}_{16}$
Ilmenite	$\text{Fe}^{2+}\text{TiO}_3$
Leucosphenite	$\text{BaNa}_4\text{Ti}_2\text{B}_2\text{Si}_{10}\text{O}_{30}$
Lorenzenite	$\text{Na}_2\text{Ti}_2(\text{Si}_2\text{O}_6)\text{O}_3$
Monazite-(Ce)	$\text{Ce}(\text{PO}_4)$
Narsarsukite	$\text{Na}_4(\text{Ti,Fe})_2[\text{Si}_8\text{O}_{20}](\text{O,OH,F})_2$
Neptunite	$\text{Na}_2\text{KLiFe}^{2+}_2\text{Ti}_2\text{Si}_8\text{O}_{24}$
Pectolite	$\text{NaCa}_2\text{Si}_3\text{O}_8(\text{OH})$
Fluorapatite	$(\text{Na,Pb,C a,REE,U})_2\text{Nb}_2\text{O}_6\text{F}$
Thorite	ThSiO_4
Titanite	$\text{CaTi}(\text{SiO}_4)\text{O}$

Table 3. Other accessory minerals identified in the Green Granite.

zenite, monazite-(Ce), narsarsukite, neptunite, pectolite, pyrochlore, thorite, titanite, zircon, and five unidentified phases. Fluorite is the most abundant accessory mineral, comprising 0.2 modal % of the whole-rock. An analysis of the granite is presented in Table 2. The Peralkalinity Index (mol. $(\text{Na}_2\text{O}+\text{K}_2\text{O})/\text{Al}_2\text{O}_3$) is 1.2 but the value may have been lowered by Na loss



Text-fig. 2. Chondrite-normalized REE plot for the Green Granite. Data from Table 2. Normalizing factors from Sun and McDonough (1989).

during post-emplacement crystallization and fluid loss. Judging from the Al_2O_3 and FeO^* contents, the magma was comenditic (Macdonald 1974). There are the high concentrations of Rb, Li, Be, Th, U, REE, Y, Zr, Hf, Nb, Ta, Sn, Zn, and F, and relatively low abundances of Ba, Sr, Cu, Co and Ni, typical of peralkaline silicic rocks. The chondrite-normalized pattern (Text-fig. 2) shows distinct LREE enrichment ($[\text{La}/\text{Yb}]_{\text{CN}} = 12.3$; where CN is chondrite-normalized) and there is a marked negative Eu anomaly ($\text{Eu}/\text{Eu}^* = 0.17$).

Analysis no.	1	2	3	4	5	6	7	8	9	10	11	11	12
	IL-6	IL-7	IL-147	IL-148	IL-149	IL-150	IL-157b	IL-306	IL-321	IL-353	IL-356	IL-8	IL-157
wt.%													
P_2O_5	b.d.	b.d.	b.d.	b.d.	b.d.	b.d.	–	–	–	0.05	0.09	b.d.	b.d.
Nb_2O_5	b.d.	0.15	–	–	–	–	0.28	b.d.	1.23	0.57	0.27	b.d.	–
Ta_2O_5	–	–	–	–	–	–	–	–	–	0.64	0.60	–	–
SiO_2	63.75	46.95	67.52	66.83	65.91	65.79	65.53	52.96	67.31	66.33	63.97	34.20	35.78
TiO_2	b.d.	0.09	b.d.	0.18	0.21	0.66	0.12	b.d.	0.33	b.d.	0.10	0.12	0.38
HfO_2	0.36	0.54	–	–	–	–	0.21	0.58	0.31	0.29	0.38	1.04	–
ThO_2	b.d.	b.d.	–	–	–	–	b.d.	–	b.d.	b.d.	b.d.	0.11	b.d.
UO_2	0.15	0.20	–	–	–	–	0.18	0.11	b.d.	0.24	b.d.	0.29	0.09
ZrO_2	20.90	33.50	16.87	17.22	17.04	17.82	17.71	31.51	19.28	17.13	16.58	54.03	57.83
La_2O_3	b.d.	b.d.	b.d.	b.d.	b.d.	b.d.	b.d.	b.d.	b.d.	–	–	0.82	0.30
Ce_2O_3	b.d.	0.15	b.d.	b.d.	0.17	b.d.	b.d.	–	b.d.	b.d.	0.09	1.13	0.38
Y_2O_3	b.d.	b.d.	2.61	1.37	1.60	0.55	1.12	0.13	b.d.	3.04	2.61	b.d.	b.d.
CaO	0.10	4.85	b.d.	0.12	0.12	0.53	0.11	0.76	0.10	0.05	b.d.	1.84	0.23
FeO^*	0.18	0.16	b.d.	b.d.	b.d.	0.18	0.05	b.d.	b.d.	b.d.	b.d.	0.15	b.d.
PbO	0.10	0.05	–	–	–	–	–	–	b.d.	–	–	0.25	b.d.
Na_2O	b.d.	b.d.	0.37	1.22	0.52	0.59	2.63	3.86	1.33	2.57	5.61	b.d.	–
K_2O	b.d.	0.05	0.71	0.42	0.61	0.14	0.20	0.05	b.d.	0.16	1.17	0.05	–
Total	85.54	86.69	88.08	87.36	86.17	86.26	88.25	89.96	90.03	91.07	91.47	94.33	95.11

Table 4. Representative compositions of secondary Zr-silicates. Explanation: Anals 1, 2, 11 – residual core (1) and mantle (2, 11) of subhedral crystal (Fig. 3d); Anals 3–6 – Fig. 3c; Anals 7, 12 – various points in bottom-left edge of aggregate in Fig. 6a; 8 – in “green zone” of Fig. 6b; 9 – in rhomb-shaped crystal (dusty blue crystal in the bottom-left corner of Fig. 6b); Anals 10, 11 – outer and inner rim of lozenge-shaped crystal (Fig. 3c); FeO^* , all Fe as Fe^{2+} . b.d. – below detection; blank – not determined. Al, Mg, Sc and V below detection in all analyses.

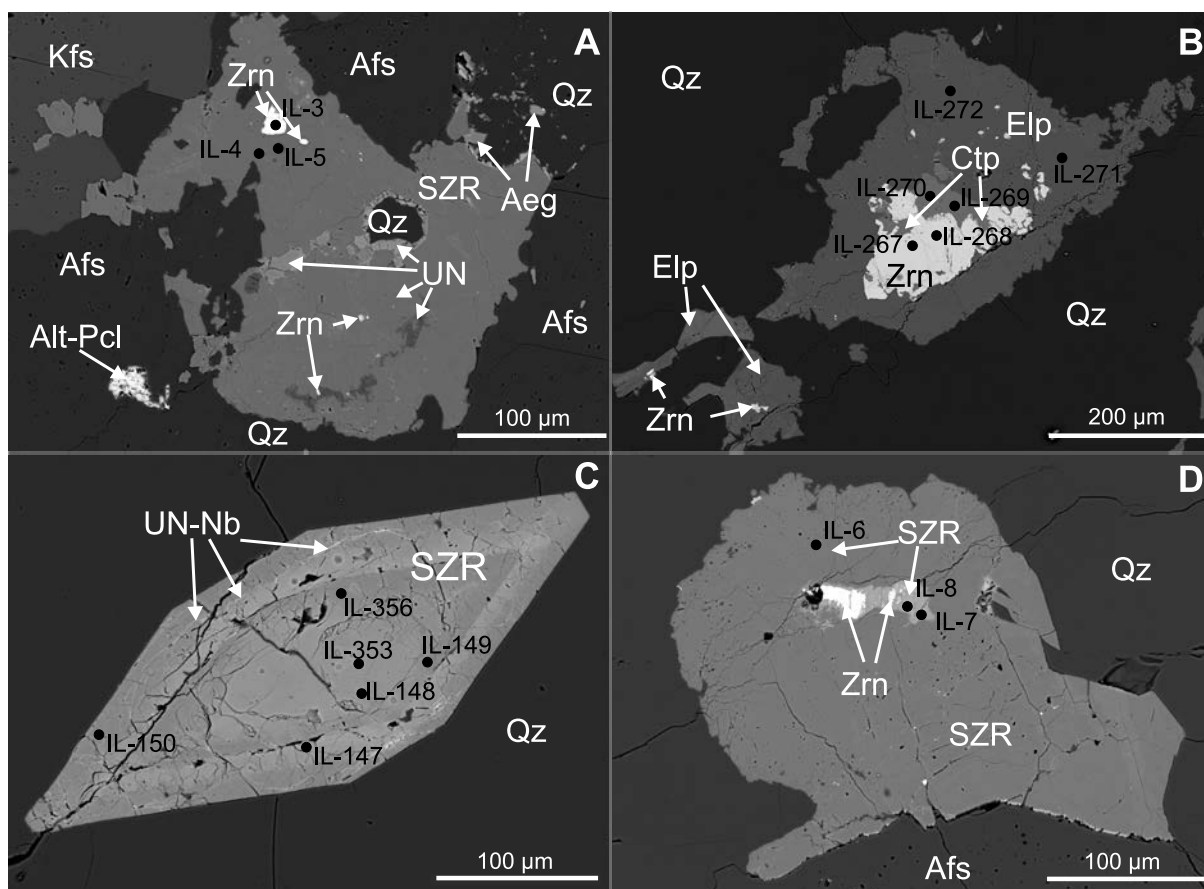
TEXTURAL RELATIONSHIPS AND COMPOSITIONS OF ZR-SILICATES

Zircon and secondary Zr-silicates

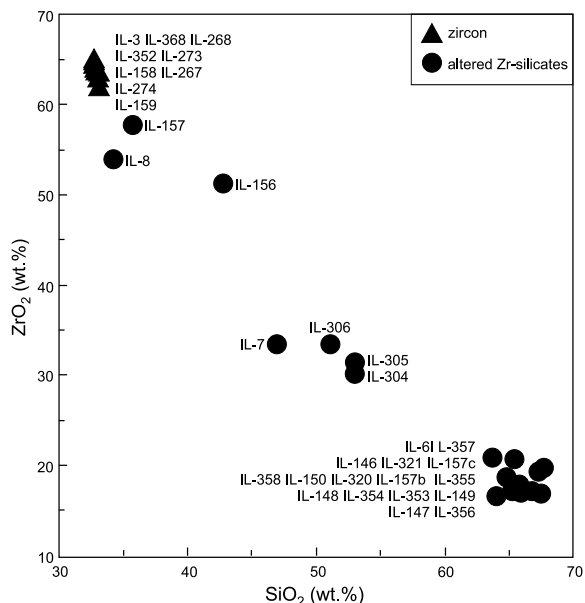
Zircon invariably occurs as partially resorbed cores within zirconosilicates (Text-fig. 3A, B). Larger crystals may have exceeded 450 μm in length. The zircon is almost perfectly stoichiometric, with $(\text{Zr}+\text{Hf}+\text{Si}) = 1.96\text{--}1.98$ a.p.f.u. and cation sums = 2.00–2.02 a.p.f.u. (Supplementary Table 1a). The only significant non-formula element is Ca, 0.003–0.019 a.p.f.u.

The term “hydrothermal zircon” has been used for zircon crystallized from, or altered by, aqueous fluids (Hoskin 2005). Hoskin and Schaltegger (2005) and Schaltegger (2007) argued that there are no textural features which unequivocally distinguish the two parageneses. Here, what we consider to be hydrothermally altered Zr-silicates, termed secondary,

are distinguished on compositional grounds; they have higher SiO_2 (35.8–63.8 wt.%) and lower ZrO_2 (20.9–57.8 wt.%) values than zircon (Text-fig. 4) and low analytical totals (85.5–95.3 wt.%; Table 4; Supplementary Table 1b). A representative example, using three analyses, from the light core and mantle of an anhedral grain (Text-fig. 3A), is presented here (Supplementary Table 1b, anals 1–3). In the sequence IL-8 through IL-7 to IL-6, SiO_2 values increase, while the contents of the other cations fall and the analytical totals decrease to 85.54 wt.%. The high CaO content in analysis IL-7 (4.85 wt.%) is anomalous in our dataset. Formulae for the secondary Zr-silicates calculated on the basis of 4 oxygens atoms show a large excess of Si (1.1–1.7 a.p.f.u.) and slightly high sums of cations (2.00–2.08 a.p.f.u.). It would appear that there is a straight replacement of Zr by Si but we have, however, no knowledge of where the excess Si may be incorporated in the structure.



Text-fig. 3. A – Residual core of zircon (Zrn) mantled by secondary Zr-silicates (SZR). B – Zircon with partial mantle of catapleite (Ctp), in turn mantled by elpidite (Elp). C – Catapleite replacing euhedral, magmatically zoned zircon. The thin white veins are an unidentified niobian phase. D – Textural relationships between secondary Zr-silicates and zircon. Compositional data for numbered points are in Supplementary Table 1b. Abbreviations: Aeg – aegirine, Afs – alkali feldspar, Alt-Pcl – altered pyrochlore, Arf – arfvedsonite, Kfs – potassium feldspar, UN-Nb – unidentified Nb-rich phase, Pcl – pyrochlore, Qz – quartz, SZR – secondary Zr-silicates, UN – unnamed Zr-silicate.



Text-fig. 4. ZrO_2 - SiO_2 plot of zircon and secondary Zr-silicates in the Green Granite. Data from Supplementary Table 1a, b.

Catapleite

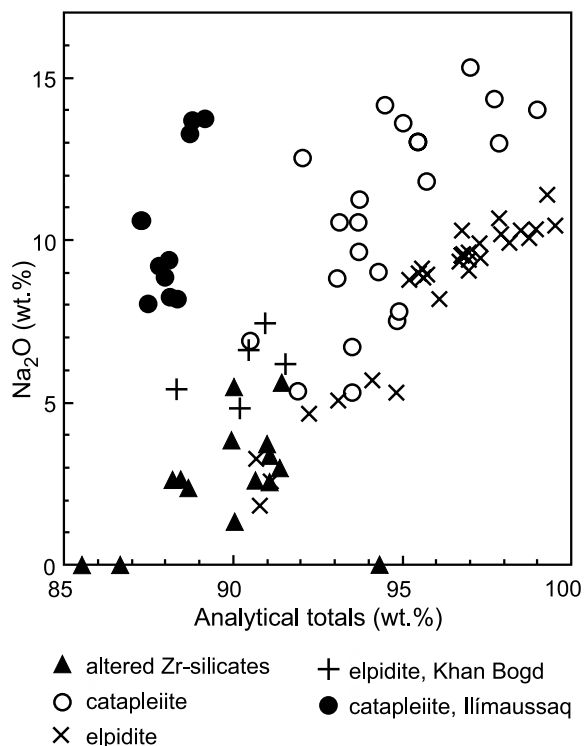
Catapleite is $[Na_2ZrSi_3O_9 \cdot 2H_2O]$ present as a partial mantle around zircon (Text-fig. 3B), as mantles around secondary Zr-silicates (Text-fig. 3D, and as patches in elpidite; Text-fig. 3B). Representative analyses are given in Table 5: the full data set is in Supplementary Table 1c. Analytical totals range from 99 to 89 wt.%; low totals have previously been recorded in catapleite by Karup-Møller *et al.* (2010) and Borst *et al.* (2016) and have been ascribed to high water contents and the possible presence of vacancies in the structure. Compositions are within the catapleite-calcic catapleite solid solution series, but CaO contents are low (≤ 1.1 wt.%). Yttrium was measured in five analyses (0.11–0.83 wt.% Y_2O_3) but no other REE were detected. The Na_2O contents range from 2.36 to 14.17 wt.%; however, values < 9 wt.% are in analyses with low analytical totals (≤ 96 wt.%) (Text-fig. 5) and low cation sums (≤ 5.2 a.p.f.u.) and it is probable that some Na was removed by hydrothermal fluids (see below).

Elpidite

Elpidite $[(Na_2ZrSi_6)O_{15} \cdot 3H_2O]$ mantles zircon, with an intermediate zone of catapleite (Text-fig. 3B), replaces euhedral magmatic zircons (Text-fig. 6A), and forms a broad mantle round the complex aggregate zone in Text-fig. 6B. Representative analyses are given in Table 6; the full data set is in Supplementary Table 1d. The analytical totals range from 91.1–99.6 wt.%. Those with the lowest totals have the lowest Na_2O contents which are inferred to be a result of hydrothermal alteration (Text-fig. 5). Calcium contents are low, ≤ 0.3 wt.% CaO.

Discussion: hydrothermal fluids

Textural evidence, low analytical totals and non-stoichiometric formulae strongly suggest that the secondary zirconosilicates, catapleite and elpidite have been altered by hydrothermal fluids. For example, loss of Na was described by Borst *et al.* (2016) in catapleite in Ilímaussaq kakortokites; in this case, during hydrothermal alteration Na was partly replaced by Ca. Karup-Møller *et al.* (2010) also found a negative relationship between Ca and Na in catapleite formed by the breakdown of eudialyte in marginal pegmatites of the Ilímaussaq complex by late-magmatic interstitial fluids. A deficiency in Na has also been reported by Salvi and Williams-Jones (1995) in elpidite in granites from Strange Lake and by Kynicky *et*



Text-fig. 5. Analytical totals plotted against Na_2O in catapleite and elpidite. Data from Supplementary Table 1c, d. Shown for comparison are elpidites from peralkaline granites of the Khan Bogd complex (Kynický *et al.* 2011) and catapleites in Ilímaussaq kakortokites (Borst *et al.* 2016).

Analysis no.	1	2	3	4	5	6	7	8
	IL-269	IL-270	IL-308	IL-312	IL-313	IL-373	IL-375	IL-366
wt. %								
P ₂ O ₅	b.d.	b.d.	–	–	–	0.19	0.17	0.23
Ta ₂ O ₅	–	–	–	–	–	0.53	0.64	0.52
SiO ₂	50.20	50.29	52.67	49.47	52.39	50.88	50.85	52.05
HfO ₂	0.55	0.47	0.72	0.63	0.58	1.01	0.65	0.66
UO ₂	0.13	0.06	b.d.	0.13	0.11	b.d.	b.d.	b.d.
ZrO ₂	29.79	30.42	30.46	31.47	30.24	32.57	35.52	33.25
Y ₂ O ₃	0.83	0.51	b.d.	b.d.	b.d.	b.d.	b.d.	b.d.
MgO	b.d.	b.d.	–	b.d.	b.d.	–	–	–
CaO	0.61	0.60	0.05		0.05	0.09	0.31	0.03
FeO*	0.16	0.14	b.d.	b.d.	b.d.	b.d.	0.03	0.05
Na ₂ O	10.60	11.27	11.83	15.32	14.35	9.05	5.34	6.73
K ₂ O	–	–	b.d.	b.d.	b.d.	b.d.	b.d.	b.d.
Total	93.14	93.75	95.74	97.02	97.72	94.32	93.51	93.52
Formulae on the basis of 9 oxygens								
P	0.000	0.000	–	–	–	0.010	0.009	0.012
Ta	0.000	0.000	0.000	0.000	0.000	0.008	0.009	0.008
Si	3.192	3.173	3.225	3.072	3.172	3.194	3.209	3.253
Hf	0.010	0.008	0.013	0.011	0.010	0.018	0.012	0.012
U	0.002	0.001	0.000	0.002	0.001	0.000	0.000	0.000
Zr	0.924	0.936	0.910	0.953	0.893	0.997	1.093	1.014
Y	0.028	0.017	0.000	0.000	0.000	0.000	0.000	0.000
Mg	0.000	0.000	0.000	0.000	0.000	–	–	–
Ca	0.041	0.041	0.006	0.000	0.004	0.006	0.021	0.002
Fe ²⁺	0.008	0.008	0.000	0.000	0.000	0.000	0.002	0.003
Na	1.307	1.379	1.405	1.845	1.685	1.101	0.653	0.816
K	–	–	0.000	0.000	0.000	0.000	0.000	0.000
Σ cations	5.51	5.56	5.56	5.88	5.77	5.34	5.01	5.12

Table 5. Representative compositions of catapleiite and altered catapleiite. Explanation: Anals 1,2 – mantling zircon (Fig. 3b); anals 3–8 – all points in catapleiite patches in Fig. 6A and B. FeO*, all Fe as Fe²⁺. bd, below detection. Dash, not determined. Al, K, La, Pb, Sc and V below detection in all analyses.

al. (2011) in elpidite from peralkaline granites from the Khan Bogd complex, southern Mongolia. In both cases, and in contrast to the Green Granite, the Na was replaced by Ca during hydrothermal alteration. Text-figure 5 shows the extent of the inferred Na loss from catapleiite and elpidite (maximum ~65% in both cases), along with examples from the literature.

The most direct evidence for the nature of the late- and post-magmatic fluids during formation of the zirconosilicates is provided by the study of fluid inclusions in quartz by Konnerup-Madsen and Rose-Hansen (1984). The fluids were entirely aqueous, with salinities between 2 and 64 wt.% and the inclusions were judged to be of post-magmatic origin. Scaillet and Macdonald (2003) and Di Carlo *et al.* (2010) showed that there is a positive correlation between CaO in amphibole and melt water content. Applying the relationship to the Green Granite is hampered by the fact that the arfvedsonites show a range of CaO contents, 0.5–2.0 wt% (our unpublished data). That

range, however, indicates a maximum water content of ~2 wt%; such a low value suggests that the melt had partially degassed at the time of titanate crystallization. Furthermore, the most abundant accessory mineral is fluorite which occurs as subhedral crystals up to 750 μm in size and as inclusions in amphibole. It is probable that it was a magmatic phase. It may be argued that crystallization of fluorite depleted the melts in F, such that late-stage fluids were F-poor, as suggested by the fluid inclusion data. Fluids enriched in Na were involved in the breakdown of zircon and formation of catapleiite and elpidite. The Na may have been released during perthitization of the feldspars. If the interpretation of the textural sequence given above is correct, it implies that the Na/Si ratio in the fluids was somewhat variable, either in space or time.

An unusual feature of the hydrothermal alteration is shown by the Zr/Hf ratios. Hf enrichment under hydrothermal conditions is well documented in zircons from LCT-family pegmatites (e.g. Neves

Analysis no.	1	2	3	4	5	6	7	8	9
	IL-272	IL-279	IL-318	IL-319	IL-325	IL-330	IL-333	IL-356	IL-370
wt. %									
P ₂ O ₅	b.d.	b.d.	–	–	–	–	–	0.09	0.11
Nb ₂ O ₅	b.d.	0.48	1.19	0.12	1.56	0.23	b.d.	0.27	b.d.
Ta ₂ O ₅	–	–	–	–	–	–	–	0.6	0.60
SiO ₂	66.34	65.70	67.69	64.77	67.06	67.04	66.71	63.97	65.21
TiO ₂	0.07	0.18	0.35	0.11	0.39	0.10	0.101	0.1	bd
HfO ₂	0.40	0.27	0.37	0.22	0.30	0.40	0.46	0.38	0.31
UO ₂	b.d.	b.d.	b.d.	0.15	–	–	–	b.d.	b.d.
ZrO ₂	20.78	19.31	17.16	19.73	17.60	19.36	20.21	16.58	21.25
V ₂ O ₃	–	–	–	–	0.11	b.d.	0.22	–	–
Ce ₂ O ₃	0.15	b.d.	–	–	–	–	–	0.09	b.d.
Y ₂ O ₃	b.d.	0.18	b.d.	1.05	b.d.	b.d.	b.d.	2.61	b.d.
MgO	0.03	b.d.	–	–	–	–	–	–	–
CaO	0.10	0.20	0.15	0.09	0.14	0.07	0.09	b.d.	0.07
FeO*	b.d.	b.d.	0.16	b.d.	b.d.	b.d.	b.d.	b.d.	0.03
PbO	b.d.	0.09	–	–	–	–	–	–	–
Na ₂ O	8.23	8.80	9.59	9.16	11.41	10.68	9.47	5.61	4.66
K ₂ O	–	–	0.10	0.22	0.06	b.d.	0.04	1.17	b.d.
Total	96.10	95.21	96.76	95.59	99.31	97.88	97.30	91.47	92.24
Formulae on the basis of 15 oxygens									
P	0.000	0.000	–	–	–	–	–	0.004	0.009
Nb	0.000	0.020	0.049	0.005	0.064	0.010	0.000	0.012	0.000
Si	6.162	6.155	6.196	6.102	6.089	6.130	6.135	6.247	6.247
Ti	0.005	0.013	0.024	0.007	0.026	0.007	0.007	0.007	0.000
Hf	0.011	0.007	0.010	0.006	0.008	0.010	0.012	0.011	0.008
U	0.000	0.000	0.000	0.003	0.000	0.000	0.000	–	0.000
Zr	0.941	0.882	0.766	0.906	0.779	0.864	0.906	0.789	0.993
V	–	–	–	–	0.008	0.000	0.016	–	0.000
Ce	0.005	0.000	0.000	0.000	0.000	0.000	0.000	0.003	0.000
Y	0.000	0.009	0.000	0.052	0.000	0.000	0.000	0.136	0.000
Mg	0.004	0.000	–	–	–	–	–	–	–
Ca	0.010	0.020	0.014	0.009	0.014	0.007	0.009	–	0.007
Fe ²⁺	0.000	0.000	0.012	0.000	0.000	0.000	0.000	0.000	0.002
Pb	0.000	0.002	–	–	–	–	–	–	–
Na	1.482	1.599	1.702	1.673	2.009	1.893	1.688	1.062	0.866
K	–	–	0.012	0.026	0.007	0.000	0.005	0.146	0.000
Σ cations	8.62	8.71	8.79	8.79	9.00	8.92	8.78	8.42	8.13

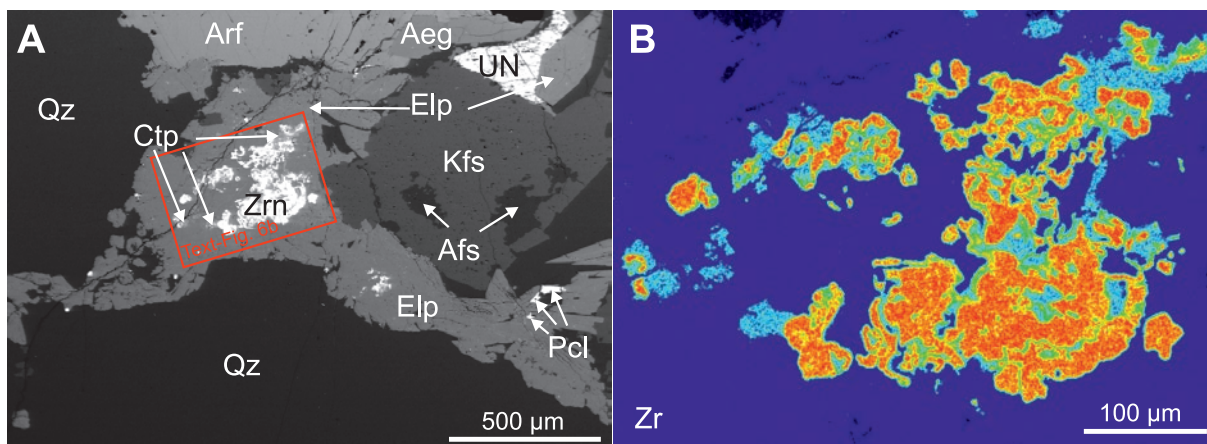
Table 6. Representative compositions of elpidite and altered elpidite. Explanation: Anal. 1, mantling zircon (Fig. 3b); anals 2–9, various points in elpidite zone in Fig. 6b. FeO*, all Fe as Fe²⁺. b.d. Below detection. Blank, not determined. Al, Cl, F, La, Sc and Th below detection in all analyses.

et al. 1974; Jacobsen *et al.* 2007; Yin *et al.* 2013; Kudryashov *et al.* 2020). This fractionation of Hf from Zr at the late hydrothermal stages has been linked to the lower mobility of Hf (Gerasimovskiy *et al.* 1972; Smith *et al.* 1987; Wang *et al.* 2010). Fractionation of Zr from Hf in the Green Granite zirconosilicates was muted: the ranges (and averages) in the different species are: zircon, 71–108 (84); secondary zirconosilicates 72–142 (99); catapleiite 71–111 (85); and elpidite 59–185 (87). This can probably be ascribed to the complicating effects of the partitioning of Zr and Hf into the other accessory phases,

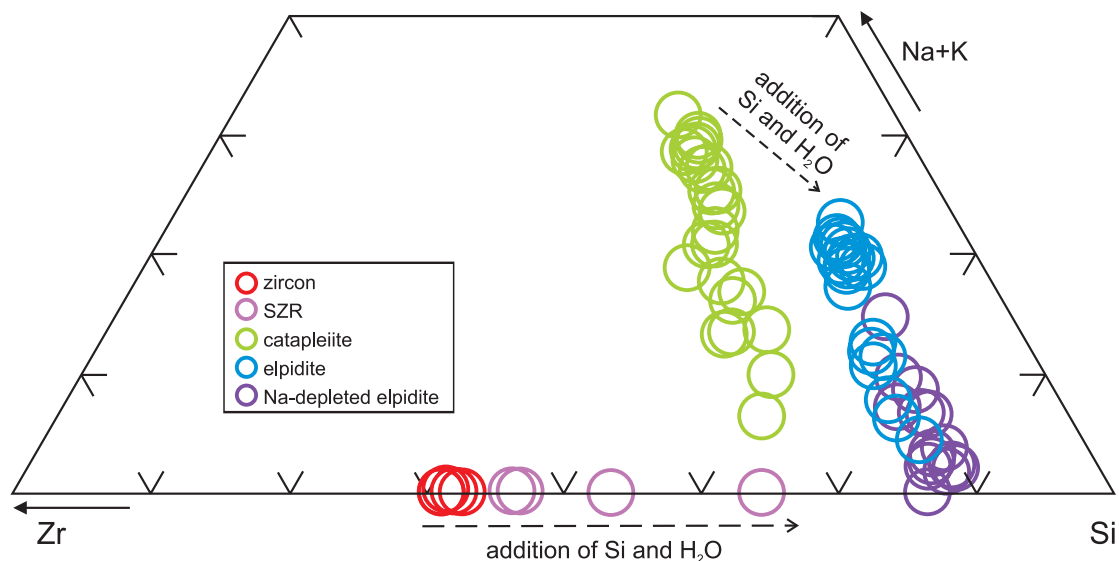
e.g. chevkinite-(Ce), leucosphenite, narsarsukite and titanite (our unpublished data).

Possible evolutionary model

The textural relationships between the phases are summarized in Text-fig. 6, which shows the clustered aggregate of phases featured in Text-fig. 3D. The red and orange areas are unaltered zircon, mantled by a green component which is altered catapleiite. Catapleiite forms the spotty light-blue areas. All are enclosed in elpidite (deep blue). These, and other, tex-



Text-fig. 6. Map of Zr distribution (B) in part of the area shown in A. Zircon – red; green – altered catapleiite; dusty blue – catapleiite; deep blue – elpidite. Abbreviations: Aeg – aegirine, Afs – alkali feldspar, Alt-Pcl – altered pyrochlore, Arf – arfvedsonite, Kfs – potassium feldspar, UN-Nb – unidentified Nb-rich phase, Pcl – pyrochlore, Qz – quartz, SZR – secondary Zr-silicates, UN – unnamed Zr-silicate.

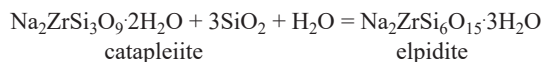


Text-fig. 7. Compositions of zircon, secondary Zr-silicates, catapleiite and elpidite plotted in a (Na+K) – Zr – Si diagram (in wt.%).

tural features allow us to speculate on the formation stages of the various phases. Zircon occurs mainly as relict cores altered into secondary zirconosilicates (Text-figs. 3, 6A), while the perfectly euhedral form and magmatic zonation of zirconosilicate pseudomorphs after zircon (Text-fig. 3C) show that at least some of the pre-alteration zircon originated during the primary magmatic stage. Catapleiite and elpidite form large crystals enclosing zircon (Text-figs. 3, 6); we interpret these as late magmatic. The hydrous alteration phase removing Na from elpidite and catapleiite is taken to be post-magmatic.

The possible relationships between the various

Zr phases may be as shown on Text-fig. 7. Initially, there was significant addition of Si and zircon was replaced by secondary zirconosilicates. There was then major addition of Na, producing catapleiite. It was then followed by a significant addition of Si and H₂O generating elpidite, a sequence consistent with the textural relationship shown in Text-figs. 3B and 6.



A later stage of hydrothermal activity partially removed Na from both catapleiite and elpidite, giving the trends away from Na (Text-fig. 7).

Acknowledgements

We thank Bruno Scaillet and Pavel Uher for helpful reviews of the manuscript. We would like to thank Beata Marciniak-Maliszewska for assistance with EPMA analyses. The first author would also like to thank Anna Harry and Paweł Jamróz for the continuous support throughout the years of research. This research was funded by the Faculty of Geology/IGMiP project 501 D-113 01 113 01 00.

REFERENCES

- Andreeva, I.A. 2016. Genesis and mechanisms of formation of rare-metal peralkaline granites of the Khaldzan Buregtey massif, Mongolia: evidence from melt inclusions. *Petrology*, **24**, 462–476.
- Borst, A.M., Friis, H., Andersen, T., Nielsen, T.F.D., Wright, T.E. and Smit, M.A. 2016. Zirconosilicates in the kakortokites of the Ilímaussaq complex, South Greenland: Implications for fluid evolution and high-field-strength and rare-earth mineralization in agpaitic systems. *Mineralogical Magazine*, **80**, 5–30.
- Di Carlo, I., Rotolo, S.G., Scaillet, B., Buccheri, V. and Pichavant, M. 2010. Phase equilibrium constraints on pre-eruptive conditions of recent felsic explosive volcanism at Pantelleria Island, Italy. *Journal of Petrology*, **51**, 2245–2276.
- Estrade, G., Salvi, S. and Béziat, D. 2018. Crystallization and destabilization of eudialyte-group minerals in peralkaline granite and pegmatite: a case study from the Ambohimirahavavy complex, Madagascar. *Mineralogical Magazine*, **82**, 375–399.
- Gerasimovskiy, V.I., Nesmeyanova, L.I., Kakhana, M.M. and Khazizova, V.D. 1972. Trends in the Zr and Hf distributions for lavas of the East African Rift zones. *Geochemistry*, **12**, 1078–1086.
- Hamilton, E.I. 1964. The geochemistry of the northern part of the Ilímaussaq intrusion, S.W. Greenland. *Grønlands Geologiske Undersøgelse Bulletin*, **42**, 104 pp.
- Hoskin, P.W.O. 2005. Trace-element composition of hydrothermal zircon and the alteration of Hadean zircon from the Jack Hills, Australia. *Geochimica et Cosmochimica Acta*, **69**, 637–648.
- Hoskin, P.W.O. and Schaltegger, U. 2005. The composition of zircon and igneous and metamorphic petrogenesis. In: J.M. Hancher and P.W.O. Hoskin (Eds), *Zircon. Reviews in Mineralogy and Geochemistry*, **53**, 2–62.
- Jacobsen, M.I., Reeve, J., Koepke, S. and Perera, N. 2007. Pegmatite mineralogy of Western Australia. *Mineral Records*, **38**, 319.
- Karup-Møller, S., Rose-Hansen, J. and Sørensen, H. 2010. Eudialyte decomposition minerals with new hitherto undescribed phases from the Ilímaussaq complex, South Greenland. *Bulletin of the Geological Society of Denmark*, **58**, 75–88.
- Kempe, U., Möckel, R., Graupner, T., Kynicky, J. and Dombon, E. 2015. The genesis of Zr-Nb-REE mineralisation at Khalzan Buregte (Western Mongolia) reconsidered. *Ore Geology Reviews*, **64**, 602–625.
- Konnerup-Madsen, J. and Rose-Hansen, J. 1984. Composition and significance of fluid inclusions in the Ilímaussaq peralkaline granite, South Greenland. *Bulletin de Minéralogie*, **107**, 317–326.
- Krumrei, T.V., Villa, I.M., Marks, M. and Markl, G. 2006. A $^{40}\text{Ar}/^{39}\text{Ar}$ and U/Pb isotopic study of the Ilímaussaq complex, South Greenland: implications for the ^{40}K decay constant and for the duration of magmatic activity in a peralkaline complex. *Chemical Geology*, **227**, 258–273.
- Kudryashov, N.M., Skublov, S.G., Galankina, O.L., Udoratina, O.V. and Voloshin A.V. 2020. Abnormally high-hafnium zircon from rare-metal pegmatites of the Vasin-Mylk deposit (the northeastern part of the Kola Peninsula). *Geochemistry*, **80**, 125489. <https://doi.org/10.1016/j.geoch.2018.12.001>.
- Kynický, J., Chakmouradian, A.R., Xu, C., Krmíček, L. and Galiova, M. 2011. Distribution and evolution of zirconium mineralization in peralkaline granites and associated pegmatites of the Khan Bogd complex, southern Mongolia. *The Canadian Mineralogist*, **49**, 947–965.
- Macdonald, R. 1974. Nomenclature and petrochemistry of the peralkaline oversaturated volcanic rocks. *Bulletin Volcanologique*, **38**, 498–516.
- Marks, M. A.W. and Markl, G. 2015. The Ilímaussaq Alkaline Complex, South Greenland. In: B. Chalié, O. Namur, R. Latypov and C. Tegner (Eds), *Silicate Liquid immiscibility in Layered Intrusions*, 649–691, Springer Geology; Dordrecht.
- Merlet, C. 1994. An accurate computer correction program for quantitative electron probe microanalysis. *Microchimica Acta*, **114/115**, 363–376.
- Neves, J.C., Nunes, J.L. and Sahama, T.G. 1974. High hafnium members of the zircon-hafnion series from the granite pegmatites of Zambesia, Mozambique. *Contributions to Mineralogy and Petrology*, **48**, 73–80.
- Salvi, S. and Williams-Jones, A.E. 1995. Zirconosilicate phase relations in the Strange Lake (Lac Brisson) pluton, Quebec-Labrador, Canada. *American Mineralogist*, **80**, 1031–1040.
- Scaillet, B. and Macdonald, R. 2003. Experimental constraints on the relationships between peralkaline rhyolites of the Kenya Rift Valley. *Journal of Petrology*, **44**, 1867–1894.
- Schaltegger, U. 2007. Hydrothermal zircon. *Elements*, **3** (1), 51, 79.
- Smith, P.E., Tatsumoto, M. and Farquhar, R. 1987. Zircon Lu-Hf systematics and evolution of the Archean crust in the southern Superior Province, Canada. *Contributions to Mineralogy and Petrology*, **97**, 93–104.

- Sørensen, H. 2006. The Ilímaussaq alkaline complex, South Greenland. An overview of 200 years of research and an outlook. *Geoscience*, **45**, 1–70.
- Sørensen, H., Bohse, H. and Bailey, J.C. 2006. The origin and mode of emplacement of lujavrites in the Ilímaussaq alkaline complex, South Greenland. *Lithos*, **91**, 286–300.
- Steenfelt, A. 1981. Field relations in the roof zone of the Ilímaussaq intrusion with special reference to the position of the alkali acid rocks. *Rapport Grønlands Geologiske Undersøgelse*, **103**, 43–52.
- Sun, S.S. and McDonough, W.F. 1989. Chemical and isotopic systematics of oceanic basalts: implications for mantle composition and processes. In: A.D. Saunders and M.J. Norry (Eds), *Magmatism in the Ocean Basins. Special Publication of the Geological Society*, **42**, 313–345.
- Upton, B.G.J. 2013. Tectono-magmatic evolution of the younger Gardar southern rift, South Greenland. *Geological Survey of Denmark and Greenland Bulletin*, **29**, 124 pp.
- Wang, X., Griffin, W. L. and Chen, J. 2010. Hf contents and Zr/Hf ratios in granitic zircons. *Geochemical Journal*, **44**, 65–72.
- Yin, R., Wang, R.C., Zhang, A.C., Hu, H., Zhu, J.C., Rao, C. and Zhang, H. 2013. Extreme fractionation from zircon to hafnon in the Koktokay No. 1 granitic pegmatite, Altai, northwestern China. *American Mineralogist*, **98**, 1714–1724.

Manuscript submitted: 28th September 2021

Revised version accepted: 15th February 2022